

# Watt-level and sub-100-fs self-starting mode-locked 2.4- $\mu\text{m}$ Cr:ZnS oscillator enabled by GaSb-SESAMs

A. BARH,<sup>\*</sup>  J. HEIDRICH,  B. O. ALAYDIN,  M. GAULKE, M. GOLLING, C. R. PHILLIPS,  AND U. KELLER 

*Department of Physics, Institute of Quantum Electronics, ETH Zurich, CH-8093, Switzerland*

*\*ajbarh@phys.ethz.ch*

**Abstract:** Femtosecond lasers with high peak power at wavelengths above 2  $\mu\text{m}$  are of high interest for generating mid-infrared (mid-IR) broadband coherent light for spectroscopic applications.  $\text{Cr}^{2+}$ -doped ZnS/ZnSe solid-state lasers are uniquely suited since they provide an ultra-broad bandwidth in combination with watt-level average power. To date, the semiconductor saturable absorber mirror (SESAM) mode-locked Cr:ZnS(e) lasers have been severely limited in power due to the lack of suitable 2.4- $\mu\text{m}$  SESAMs. For the first time, we develop novel high-performance 2.4- $\mu\text{m}$  type-I and type-II SESAMs, and thereby obtain state-of-the-art mode-locking performance. The type-I InGaSb/GaSb SESAM demonstrates a low non-saturable loss (0.8%) and an ultrafast recovery time (1.9 ps). By incorporating this SESAM in a 250-MHz Cr:ZnS laser cavity, we demonstrate fundamental mode-locking at 2.37  $\mu\text{m}$  with 0.8 W average power and 79-fs pulse duration. This corresponds to a peak power of 39 kW, which is the highest so far for any saturable absorber mode-locked Cr:ZnS(e) oscillator. In the same laser cavity, we could also generate 120-fs pulses at a record high average power of 1 W. A comparable laser performance is achieved using type-II InAs/GaSb SESAM as well. These results pave the way towards a new class of high-power femtosecond SESAM mode-locked oscillators operating directly above 2- $\mu\text{m}$  wavelength.

© 2021 Optical Society of America under the terms of the [OSA Open Access Publishing Agreement](#)

## 1. Introduction

Broadband laser sources in the short-wave infrared (SWIR) spectral region, with wavelengths between 2–3  $\mu\text{m}$ , are attractive for diverse applications. Such SWIR sources can directly be used for spectroscopic monitoring of atmospheric trace gases, remote sensing, laser ranging (LIDAR), free-space communication [1–3], and for driving various nonlinear processes, e.g. long-wave infrared supercontinuum generation, difference frequency generation, optical parametric amplification, and high-harmonic generation [4,5]. Due to the longer center wavelength compared with traditional fs-lasers in the near-infrared (near-IR), fs 2- $\mu\text{m}$  lasers are compatible with non-oxide nonlinear materials such as AGSe, CdSe, ZGP, GaSe, and OP- GaAs [6–8] which enable efficient frequency conversion to the important molecular fingerprint spectral region [7–10].

Optically pumped transition metal ( $\text{Cr}^{2+}$ ) doped ZnS/ZnSe solid-state lasers (SSLs), hereafter referred to collectively as Cr:ZnS(e), have shown wide wavelength tunability covering the entire 2–3  $\mu\text{m}$  range [11,12] with high power operation [13,14]. The vibronic laser transition of such gain media provides wide gain bandwidth,  $\mu\text{s}$ -range upper state lifetime, no excited state absorption, room temperature operation, and close to a four-level energy structure. Additionally, they can be pumped with high brightness fiber lasers at 1.55  $\mu\text{m}$  (Er: fiber) or 1.95  $\mu\text{m}$  (Tm: fiber) for quality output. Hence, these materials offer very similar advantages for fs-lasers in the 2 – 3  $\mu\text{m}$  spectral range as Ti:sapphire offers in the near-IR [12].

Femtosecond Cr:ZnS(e) oscillators commonly rely on either Kerr-lens [13] or real saturable absorber based passive mode-locking schemes [15,16]. Though the first fs Cr:ZnS(e) oscillator was reported in 2005 [17] by using a semiconductor saturable absorber mirror (SESAM) [18], the current state-of-the-art performance is achieved mainly by using Kerr-lens mode-locking (KLM) [13,19–21]. While KLM is ideal for generating few-cycle pulses [13,19–21], SESAM mode-locking offers several other advantages. SESAMs are widely known for enabling low-noise and self-starting mode-locked lasers, while using robust laser cavities operated in the middle of their stability zone. Moreover, they support a wide range of repetition rates [22,23] as well as high average power [24].

Achieving short recovery times, low non-saturable losses, and suitable modulation depths is crucial for high-performance SESAM mode-locked lasers [18,25]. However, until now the performance of 2.4- $\mu\text{m}$  SESAMs has been lacking. Based on the semiconductor band alignment of the absorber section of a SESAM, it can be categorized in two types, type-I and type-II [26,27]. So far the only SESAM reported for mode-locking of Cr:ZnS(e) oscillators is a type-II InAs/GaSb superlattice SESAM [17,28]. Full optical characterization of the SESAM was never performed, but it had a high small-signal absorption loss of  $\sim 12\%$  per reflection and an estimated recovery time on the order of a nanosecond (ns). The lack of suitable mid-infrared (mid-IR) SESAMs severely limited the performance of these Cr:ZnS(e) oscillators. A major challenge of mid-IR quantum well (QW)-based SESAM development is that it relies on the GaSb optoelectronic platform, which is much less mature than the conventional InGaAs platform used for near-IR SESAMs.

Here we address this challenge by developing for the first time a low-loss and high-speed type-I InGaSb/GaSb QW-based SESAM at  $\sim 2.35 \mu\text{m}$ . The low non-saturable losses (0.8%) and ultrafast absorber recovery time (1.9 ps) of the SESAM enable a stable mode-locking and allow to reach high power level even with a relatively low 5% output coupler. With this SESAM we demonstrate self-starting mode-locking of a Cr:ZnS oscillator with a repetition rate of 250 MHz delivering average power up to 1 W and pulse durations as short as 79 fs. In a first configuration, we obtain 79 fs full-width at half maximum (FWHM) pulses with 0.8 W average power at 2366 nm. In a second configuration, we obtain 1 W average power and 120 fs pulse duration at 2373 nm. Moreover, as part of our investigation into 2.4- $\mu\text{m}$  SESAMs, we developed a state-of-the-art type-II InAs/GaSb multi-QW SESAM with low non-saturable losses of 0.5%. With that device, we obtain similar average power of 0.93 W, with slightly longer pulses of 168 fs.

To the best of our knowledge, our results represent the first SESAM mode-locked Cr:ZnS oscillator with (i) watt-level output power and (ii) sub-100-fs optical pulses. In particular, these results represent more than 5-fold increase in both average and peak power than previously demonstrated SESAM mode-locked fs-Cr:ZnS oscillators [15]. Moreover, we demonstrate (iii) the longest wavelength type-I QW SESAM-based any ultrafast laser, and (iv) first watt-class output power from a fs-Cr:ZnS oscillator using a type-II InAs/GaSb multi-QW SESAM.

The article is organized as follows. In section 2, we present the macroscopic optical properties of the two types of SESAM devices, type-I and type-II. In section 3, we show the laser configuration and diagnostics. In section 4, we present and discuss the mode-locking results including both the SESAMs. Finally, the paper is concluded in section 5.

## 2. 2.4- $\mu\text{m}$ SESAM devices

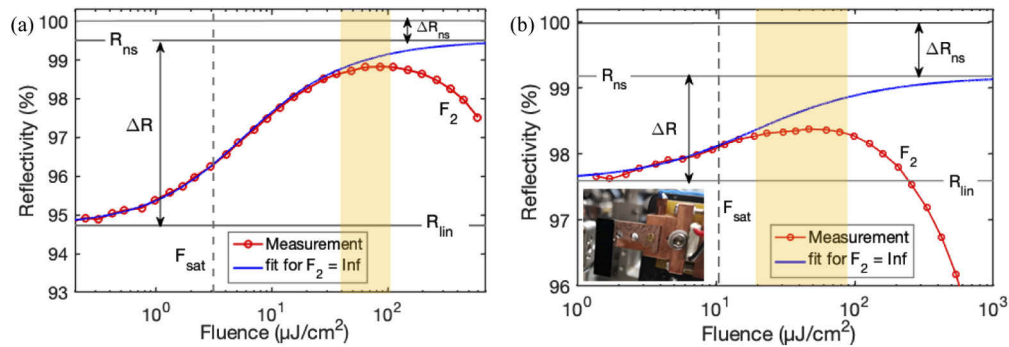
Since the invention of the SESAMs in early 1990s [18], stable passive mode-locked and Q-switched solid-state, semiconductor, and fiber lasers have become commercially available. Current high performance SESAMs are primarily based on the well-developed GaAs/InGaAs optoelectronic platform, covering the spectral range from around 800 nm to 1550 nm [29]. At wavelengths exceeding 2  $\mu\text{m}$ , most research has been focused on GaSb based material systems. Though researchers have demonstrated InGaSb/GaSb QW-based high quality SESAM at 2  $\mu\text{m}$

wavelength [30], the quality of SESAMs available at longer operating wavelengths is significantly reduced, making the oscillators less stable and of lower power level ( $< 200$  mW).

To address these issues, we developed capability to grow GaSb-based epilayers by means of molecular beam epitaxy (MBE) at the FIRST cleanroom facility at ETH Zurich in combination with systematic SESAM characterization measurements, the details of which will be presented elsewhere. In the following sub-sections, we briefly discuss the two types of SESAM devices developed within this facility for mode-locking our Cr:ZnS laser.

### 2.1. Type-II InAs/GaSb multi-QW SESAM

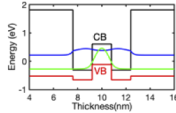
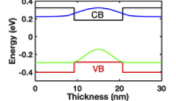
In our first growth campaign, we focused on type-II InAs/GaSb multi-QW SESAMs. The binary structures exhibit low strain and can be bandgap engineered to work over the entire 2–4.5  $\mu\text{m}$  spectral range [27]. We initially fabricated a SESAM centered around 2.35  $\mu\text{m}$ . The wavelength is chosen around the peak of the Cr:ZnS gain spectrum. The SESAM consists of 20 $\times$  type-II W-like AlSb/InAs/GaSb/InAs/AlSb multi-QWs grown on 24 pair of AlAsSb/GaSb distributed Bragg reflector (DBR). We characterized the SESAM by using our SWIR nonlinear reflectivity measurement and pump-probe setup. The measurements are performed using a 105 fs (chirped to  $\sim 120$  fs at position of device under test) 80 MHz commercial tunable optical parametric oscillator (OPO) light source operating at  $\sim 2.36$   $\mu\text{m}$ . The nonlinear reflectivity of the SESAM is measured precisely over a high dynamic range of pulse fluence more than  $10^3$  [see Fig. 1(a)]. Using the model for SESAM saturation including roll-over effects [31,32], we find the values of saturation fluence ( $F_{\text{sat}}$ ), modulation depth ( $\Delta R$ ), non-saturable loss ( $\Delta R_{\text{ns}}$ ), and roll-over parameter ( $F_2$ ) as tabulated in Table 1. We have achieved extremely low non-saturable loss of only 0.5%. However, nonlinear absorption effects (e.g., multiphoton absorption in the GaSb layers) leads to a roll-over, which eventually the reflectivity of SESAM at higher fluences (see Fig. 1) [32].



**Fig. 1.** Nonlinear reflectivity measurement of the (a) type-II InAs/GaSb multi-QW SESAM, and (b) type-I InGaSb/GaSb QW SESAM at  $\sim 2.36$   $\mu\text{m}$ . The red circles are the measured data and the blue solid line is the fit considering no roll-over, i.e., for  $F_2 = \text{infinity}$ . Other symbols are discussed in the text. The yellow shaded area indicates our mode-locked laser operation regime as discussed in section 3 and 4. In (b) a picture of mounted type-I SESAM is displayed as inset.

The remaining drawback of these type-II SESAMs is their recovery time. SESAMs typically exhibit a fast and a slow recovery time, denoted by  $\tau_{\text{fast}}$  and  $\tau_{\text{slow}}$  respectively [33]. The slow recovery part can still contribute to stabilizing the soliton mode-locked state even when  $\tau_{\text{slow}}$  is of order 30 times the pulse duration of the mode-locked laser [34]. However, although we measured a  $\tau_{\text{fast}}$  of 300 fs, the  $\tau_{\text{slow}}$  was  $> 1$  ns (longer than resolvable in the measurement). Moreover, we find a normalized amplitude [33]  $A_{\text{slow}}$  of  $\sim 0.58$ , meaning that about 42% of the losses have

**Table 1. Macroscopic SESAM parameters measured using a  $\sim 120$  fs, 80 MHz OPO operating at  $\sim 2.36$   $\mu\text{m}$ . CB: conduction band. VB: valence band.**

SESAM parameters	$F_{\text{sat}}$ ( $\mu\text{J}/\text{cm}^2$ )	$\Delta R$ (%)	$\Delta R_{\text{ns}}$ (%)	$F_2$ ( $\text{mJ}/\text{cm}^2$ )	Absorber recovery dynamics		
					$\tau_{\text{fast}}$ (fs)	$\tau_{\text{slow}}$ (fs)	$A_{\text{slow}}$
Type-II							
	3.13	4.78	0.5	31	300	$> 10^6$	0.58
Type-I							
	10.51	1.59	0.8	18	160	1900	0.45

recovered after the fast recovery phase, while the remaining losses take  $> 1$  ns to recover. Hence, for this device, only a fraction  $(1 - A_{\text{slow}})$  of the modulation depth displayed in Table 1 is actually useful for stabilizing femtosecond mode-locking. Additionally, the long recovery time could be problematic for high repetition rate lasers due to incomplete recovery between the pulses.

## 2.2. Type-I InGaSb/GaSb QW SESAM

To obtain faster recovery dynamics, we developed a novel type-I InGaSb/GaSb QW based SESAM at  $\sim 2.36$   $\mu\text{m}$ . The SESAM consists of  $3 \times$  QWs on top of a 24 pair of AlAsSb/GaSb DBR. To the best of our knowledge, this SESAM is the first type-I SESAM that has been used to mode-locked any ultrafast laser operating at wavelength above 2  $\mu\text{m}$ . Note that, the longest operating wavelength of a laser reported so far with a type-I SESAM is a 1.96  $\mu\text{m}$  VECSEL [22,30]. To fabricate this device, we increased the indium fraction in the QW to red-shift the wavelength. Consequently, the structure has increased strain, which is a trade-off while pushing type-I InGaSb/GaSb QW devices to longer wavelength [35]. Nonetheless, we have not experienced any damage on the SESAM during laser operation. The nonlinear reflectivity measurement is shown in Fig. 1(b). The SESAM shows a remarkable set of parameters (see Table 1) with low non-saturable loss ( $\sim 0.8\%$ ) and ultrafast recovery time constants ( $\tau_{\text{fast}} \sim 160$  fs and  $\tau_{\text{slow}} \sim 1.9$  ps). The  $\tau_{\text{fast}}$  is improved by a factor of 2 compared to the type-II SESAM. Even more importantly, the  $\tau_{\text{slow}}$  is improved by at least  $500\times$ , meaning that the full  $\Delta R$  can now contribute to stabilizing femtosecond mode-locking.

Both of the SESAMs are designed as standard antiresonance configuration, and have a simulated GDD profile with  $\text{GDD} = \pm 200$  fs<sup>2</sup> over a 60 nm bandwidth centered around 2.34  $\mu\text{m}$ . Schematic semiconductor band structures of the designed SESAMs are displayed in Table 1. Note that, the measured recovery time of the 2.4- $\mu\text{m}$  type-I GaSb-based SESAM is much faster than a InGaAs-based near-IR SESAM, mainly due to the stronger Auger recombination at lower bandgap materials [35]. This favors shorter pulse formation for the Cr:ZnS oscillator which has an inherently broad gain bandwidth.

## 3. Laser setup and design

The experimental setup is depicted in Fig. 2. We used polycrystalline Cr:ZnS as gain element with a specified doping concentration of  $9.1 \times 10^{18}/\text{cm}^3$  (IPG Photonics). The gain element is 3.8 mm long, Brewster cut, and mounted on a water-cooled thermo-electric (TEC) controlled copper (Cu) mount coupled to x-y-z translation and rotation stages. A 1550 nm Er-fiber laser system (NKT Photonics) providing up to 10 watt of continuous wave (cw) output power is used for

pumping. Measured single pass absorption in the gain element at this pump wavelength is  $\sim 68\%$  and it is temperature stabilized at  $\sim 16^\circ\text{C}$ . The input coupling mirror (M1 in Fig. 2) transmits  $> 93\%$  of pump power. The gain element is placed in the middle of the first stability zone of an X-folded cavity. The SESAM, working as a flat end mirror, is mounted on a TEC controlled Cu mount and temperature stabilized at  $\sim 15^\circ\text{C}$  throughout the experiment. All the cavity turning mirrors (M1 – M5) are IBS coated for broadband high reflection (HR) over  $2.1\text{--}3.0\ \mu\text{m}$  with nearly flat group delay dispersion (GDD), however not optimized for any higher order dispersion (Optoman). For dispersion optimization in the different laser configurations, we used 6-mm-thick Brewster plates made of either YAG or Sapphire. The output coupler (OC) is IBS coated for  $5\%$  transmission over  $2.2\text{--}2.6\ \mu\text{m}$  with nearly flat GDD (U. of Neuchatel). The measured pump spot size radius at input facet of the gain element is  $\sim 40\ \mu\text{m}$ , whereas the calculated laser mode size radius is  $\sim 48\ \mu\text{m}$ . Furthermore, the astigmatism introduced by the gain element and Brewster plate is minimized by choosing incident angles on the curved mirrors between  $7^\circ\text{--}9^\circ$ . The laser is operated in a standard laboratory environment with relative humidity of  $40\text{--}60\%$ . The laser is polarized in the horizontal direction. Overall, the laser cavity design is simple and compact ( $30\ \text{cm} \times 20\ \text{cm}$  footprint).

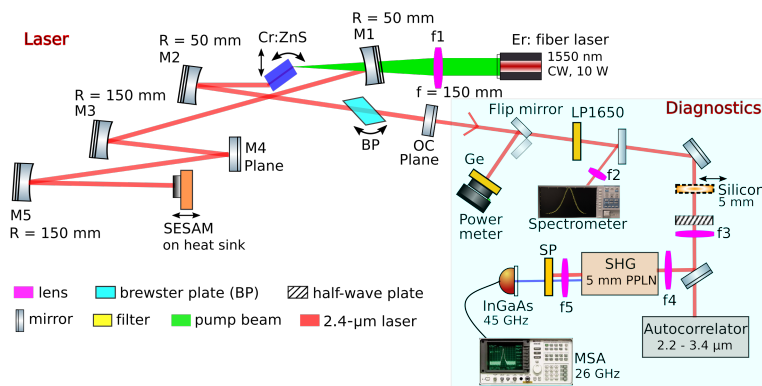


**Fig. 2.** Schematic of the Cr:ZnS laser cavity as well as the diagnostic setup (shaded area) of the  $2.4\text{-}\mu\text{m}$  laser. The ceramic Cr:ZnS and Brewster plate (BP) are mounted on translation-rotation stage to optimize the Brewster incidence for lowest loss. Mirrors M1 – M5 are coated for high transmission at  $1550\ \text{nm}$  and high reflection over  $2.1\text{--}3.0\ \mu\text{m}$ . The output coupler (OC) is  $5\%$  and made of infrared fused silica substrate. The diagnostics setup measures power, spectrum, autocorrelation, and repetition rate via extra-cavity SHG. LP: long pass, SP: short pass.

We achieve fundamental soliton mode-locking [36] in the negative (anomalous) dispersion regime by compensating intracavity nonlinear phase shift with intracavity GDD. The estimated round-trip GDD of the cavity elements and the ideal GDD for soliton condition is plotted in Fig. 3 for the highest output power configuration with the type-I SESAM. Note that, no special optics are used for higher order dispersion management. Both SESAMs have the same DBR structure behind the active QW layers. The measured reflectivity of a DBR reference sample (Fig. 3) shows  $>99.5\%$  over a  $110\ \text{nm}$  bandwidth ( $2280\text{--}2390\ \text{nm}$ ). The output coupler is flat, wedged, and has  $5\%$  transmission for the laser; this value is best suited (from our limited collection) for the available SESAM parameters.

The diagnostic arrangement is outlined in Fig. 2 as well. A large area thermal power meter (Thorlabs S425C) is used to monitoring the output power. An anti-reflection (AR) coated germanium (Ge)-window is used to block any remaining pump beam and pass only the laser light. A part of the beam reflected from a  $\text{CaF}_2$  wedge is used to measure the optical spectrum by using a grating based optical spectrum analyzer (OSA, Yokogawa AQ6376) with optical resolution set

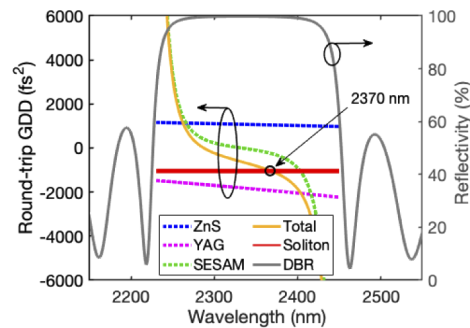


**Fig. 3.** The estimated round-trip GDD of the cavity elements and the measured reflectivity of the DBR reference sample (grey solid). The cavity consists of 6-mm YAG Brewster plate and type-I SESAM. GDD of Cr:ZnS (blue dashed), YAG (pink dashed), and SESAM (green dashed) together with total GDD (yellow solid) is plotted. The red solid is the GDD needed to satisfy the soliton condition for 120 fs pulses at 0.96 W of output power. The lasing wavelength should be centered around 2370 nm.

at 0.5 nm. The rest of the beam is directed to a mid-IR intensity autocorrelator (Femtochrome) and a home-built repetition rate measurement setup. A 5 mm thick AR-coated silicon window is used in the autocorrelator path in order to compensate for the chirp in the pulses acquired over its travel path (further discussed in the next section). One of the standard mode-locking diagnostics is a measurement of the mode-locked pulse train on a fast photodiode and microwave spectrum analyzer (MSA), thereby revealing the microwave comb structure. This measurement, together with optical spectrum and autocorrelation, validates mode-locked operation. However, because of the lack of high-speed mid-IR detectors, a direct measurement of this kind was not possible. Therefore, a second harmonic generation (SHG) based measurement was used instead. A 5-mm long periodically poled lithium niobate (PPLN) crystal is used for SHG of the laser output, and the second harmonic beam ( $\sim 1180$  nm range) is detected using a high-speed InGaAs detector (45 GHz) connected to a 26-GHz MSA.

#### 4. Mode-locking results

The best mode-locking performance is achieved while operating the SESAM in fully saturated regime with excitation fluence close to roll-over point. We could achieve watt-level output power for both type-I and type-II SESAM mode-locked cavity configurations. Note that, by replacing the SESAM with a HR mirror, we could achieve  $\sim 2$  W of average output power at 7.5 W of pump power providing 26.7% of lasing efficiency of the cavity in cw mode. In this section, we first present the mode-locking results using the type-I SESAM (where we achieved the best performance), then compare it with the laser performance using the type-II SESAM.

##### 4.1. Using type-I InGaSb/GaSb QW SESAM

With the type-I SESAM inside the cavity, we consider two cavity configurations, one for achieving lowest pulse duration (Config-I-a) and another for achieving highest output power (Config-I-b). In case of Config-I-a, the distance from mirror M5 to the SESAM (see Fig. 2) is set to 75 mm, giving laser spot size on the SESAM of  $\sim 148$   $\mu\text{m}$ . To achieve the highest power in Config-I-b, the distance is increased to 79 mm giving a laser spot size on the SESAM of  $\sim 159$   $\mu\text{m}$ . The rest of the cavity is unchanged and a 6-mm YAG is used for GDD compensation for both the configurations. Stable mode-locking operation is achieved for a fluence range of 20  $\sim$  95  $\mu\text{J}/\text{cm}^2$  on the SESAM [indicated by the yellow shaded area in Fig. 1(b)].

## 4.1.1. Config-I-a: sub-100-fs pulse duration

We observe cw operation at low pump power [blue open circle in Fig. 4(a)] and then with increasing pump power the laser reliably transitions into self-starting soliton mode-locking at around 200 mW of average output power [blue solid in Fig. 4(a)]. A stable fundamental mode-locking is achieved for average output power of  $\sim 200$ –770 mW. At higher power levels harmonic mode-locking or multi pulsing is observed. For this measurement, we have estimated that the GDD in the path of the laser beam up to the autocorrelator setup is  $\sim -3000$  fs<sup>2</sup>, which is sufficient to chirp sub-100-fs pulses significantly. By introducing a single AR-coated 5 mm thick silicon (Si) providing positive GDD in the beam path (see Fig. 2), we could achieve close to transform-limited pulses over the entire mode-locking regime [yellow solid in Fig. 4(b)]. Furthermore, the increase in bandwidth and decrease in pulse duration with respect to output power shown in Fig. 4(b) are strong indicators of a soliton mode-locking mechanism for the pulse formation [36]. The spectrum broadening with increasing pump power is displayed in Fig. 4(c). The non-uniformity in the bandwidth as well as in the pulse duration measurements [Fig. 4(b)] can be attributed to the shift in central wavelength ( $\lambda_0$ ) at different power level [inset in Fig. 4(c)] together with the limitation in the SESAM reflectivity (see Fig. 3). At the highest output power of 0.8 W, we have achieved 79 fs pulses (corresponding to 10 optical cycles), with FWHM bandwidth of  $\sim 71$  nm. The corresponding time-bandwidth product (TBP) is 0.303 (0.96 $\times$  the transform limit for an ideal sech<sup>2</sup> pulse), pulse energy is 3.1 nJ, and peak power is 39 kW. This is the highest peak power reported so far for any real saturable absorber based mode-locked Cr:ZnS(e) oscillator. The measured optical spectrum and SHG based intensity autocorrelation for this case is displayed in Figs. 4(d) and 4(e), respectively. The clean radio frequency (RF) spectrum, measured using PPLN-SHG [Fig. 4(f)], shows fundamental mode-locking operation.

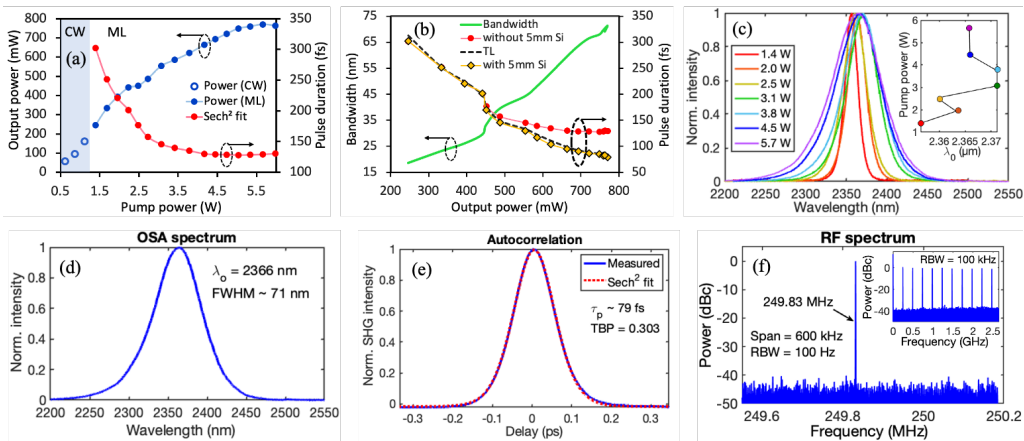


**Fig. 4.** Config-I-a: fundamental mode-locking results using type-I SESAM for shortest  $\tau_p$ . (a) Measured output power (cw: blue open circle and mode-locked (ML): blue solid circle) and sech<sup>2</sup> fitted  $\tau_p$  (red solid) as a function of incident pump power. (b) Measured FWHM bandwidth (green solid), sech<sup>2</sup> fitted  $\tau_p$  without (red solid) and with (yellow solid) 5 mm thick Si in the path, and ideal transform-limited (TL)  $\tau_p$  (grey dashed). (c) Optical spectrum at different pump powers. Inset shows variation in center wavelength ( $\lambda_0$ ), color code follows same power values as of main figure. (d)–(f) Data set for shortest pulse configuration. (d) Optical spectrum. (e) Autocorrelation trace with sech<sup>2</sup> fit. (f) RF trace with a resolution bandwidth (RBW) of 100 Hz and a span of 600 kHz showing a repetition rate of  $\sim 250$  MHz. Inset shows RF traces over a wider span (2.6 GHz) with RBW of 100 kHz.

#### 4.1.2. Config-I-b: watt-level average output power

The strong SESAM roll-over [see Fig. 1(b) and Table 1] is essentially limiting the power scaling of fundamental mode-locking for the cavity Config-I-a. One straightforward way to overcome this issue is by increasing the laser spot size on SESAM, which allows reaching the roll-over region at a higher output power. In Config-I-b, the SESAM is displaced along the cavity length by few mm in order to increase the laser spot size on it. The rest of the cavity and optics remain unchanged. We could achieve maximum fundamental mode-locking power of 0.96 W at 120 fs pulse duration [see Fig. 5(a)], corresponding to FWHM bandwidth of 50 nm, TBP of 0.319 ( $1.01\times$  the transform limit for a  $\text{sech}^2$  pulse), peak power of 32 kW, and pulse energy of 3.9 nJ. We demonstrate  $\sim 5\times$  increase in average output power and  $\sim 7\times$  increase in pulse energy compared to all previously demonstrated SESAM mode-locked fs-CrZnS(e) oscillators [15]. The measured intensity autocorrelation trace and optical spectrum are shown in Fig. 5(b). The center wavelength of emission is  $\sim 2373$  nm, which agrees well with the calculated soliton condition (see Fig. 3). The estimated intracavity pulse fluence on the SESAM is  $\sim 93 \mu\text{J}/\text{cm}^2$ . Even at this high fluence level we did not observe any damage on the SESAM. A long-term power stability for the laser operation over 3.5 hours is recorded in every 10 sec [Fig. 5(c)] using a thermal power meter (Thorlabs S425C, specified response time is 0.6 sec). A long-term drift of rms  $< 0.3\%$  (over 3.5 hours) and a short-term drift of rms  $< 0.1\%$  (over 20 min) is recorded. At this high-power level an excellent output beam quality is measured using a microbolometer based camera (WinCamD) and shown as inset in Fig. 5(c). A clean RF spectrum is measured; however, it is not shown here.

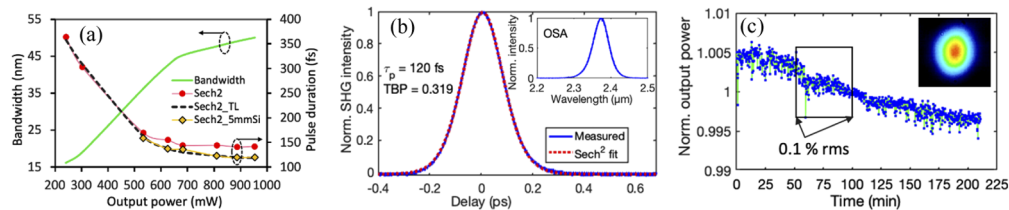


**Fig. 5.** Config-I-b: fundamental mode-locking results using type-I SESAM for highest output power. (a) Measured FWHM bandwidth (green solid), pulse duration without (red solid) and with (yellow solid) 5 mm Si, estimated ideal transform-limited (TL) pulse duration at corresponding bandwidth (grey dashed) are plotted as a function of mode-locked output power. (b) Autocorrelation trace with  $\text{sech}^2$  fit. Inset shows optical spectrum of FWHM 50 nm. (c) Output power stability over 3.5 hours. The rms power fluctuation over indicated (black square) time window is 0.1%. Inset shows measured beam profile.

## 4.2. Using type-II InAs/GaSb multi-QW SESAM

In this section, we present the mode-locking results using our low-loss type-II multi-QW SESAM. The mode-locking is self-starting, however, due to longer recovery time (ns-scale), the lasing is less stable than the type-I case (further detail in “Discussion” section). Nevertheless, we observe fundamental mode-locking over a broad power range and of fs pulse duration. We present two mode-locking configurations, one for achieving sub-100-fs pulse duration (Config-II-a) and other for achieving watt-level output power (Config-II-b).

#### 4.2.1. Config-II-a: sub-100-fs pulse duration

In this configuration, we used the 6-mm YAG as GDD compensating element inside the cavity. Fundamental mode-locking is established at output power level from 400–790 mW. The measured FWHM spectral bandwidth and pulse durations are plotted in Fig. 6(a). Similar to the previous



measurements, we use AR-coated 5 mm Si to compensate for the chirp and obtain transform-limited pulses. We have achieved 87 fs pulses [Fig. 6(b)] of 71 nm FWHM bandwidth [inset in Fig. 6(b)] at output power of  $\sim 0.75$  W. The corresponding TBP is 0.331 ( $1.04\times$  ideal  $\text{sech}^2$ ), pulse energy is 3.0 nJ, and peak power is 34.5 kW. The inset in Fig. 6(b) shows two spectra measured on the OSA, one for shortest  $\tau_p$  (blue) and the other for longest  $\tau_p$  (light blue), which indicates that the bandwidth is limited at the red-end of the spectrum and might originate from the limited SESAM bandwidth (see Fig. 3). The measured clean RF spectrum [Fig. 6(c)] shows fundamental mode-locking.

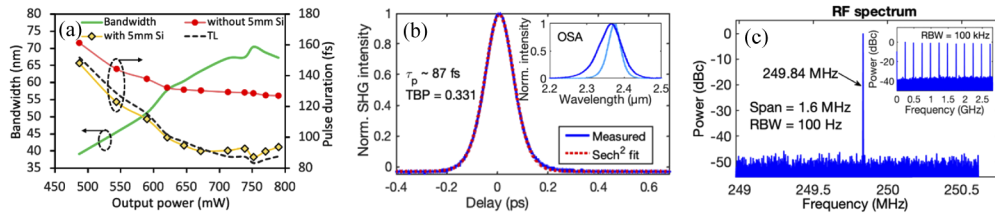


**Fig. 6.** Config-II-a: fundamental mode-locking results using type-II SESAM for shortest pulse duration. (a) Measured FWHM bandwidth (green solid),  $\tau_p$  without (red solid) and with (yellow solid) 5 mm Si in diagnostic path, estimated ideal transform-limited (TL)  $\tau_p$  at corresponding bandwidth (grey dashed) are plotted as a function of mode-locked output power. (b) Autocorrelation trace with  $\text{sech}^2$  fit. Inset shows optical spectrum for minimum  $\tau_p \sim 87$  fs (blue, FWHM of 71 nm) and for maximum  $\tau_p$  (light blue, FWHM of 39.5 nm). (c) RF trace with a resolution bandwidth (RBW) of 100 Hz and a span of 1.6 MHz showing a repetition rate of  $\sim 250$  MHz. Inset shows RF traces over a wider span (2.8 GHz) with RBW of 100 kHz.

#### 4.2.2. Config-II-b: watt-level average output power

To extract more power from the cavity and to test the fluence limit of the type-II SESAM for fundamental mode-locking, we needed to increase the GDD in the cavity in order to balance the increased intracavity nonlinearity. We have achieved it by replacing the YAG with a 6-mm Sapphire Brewster plate. The GDD coefficient of YAG and Sapphire at  $2.37 \mu\text{m}$  is  $-141.12 \text{ fs}^2/\text{mm}$  and  $-229.79 \text{ fs}^2/\text{mm}$ , respectively. Everything else is unchanged including the SESAM position. We believe that due to weaker roll-over effect (higher  $F_2$ ) for the type-II SESAM in comparison to the type-I SESAM (see Table 1), the high-power limit (Config-II-b) is more sensitive to the GDD adjustment rather than the fluence on SESAM, as we have observed previously for type-I case. Higher values of GDD lead to a blue-shift in the wavelength that satisfies the soliton formation condition. This shift ensures that the center wavelength of the soliton pulse stays within the SESAM bandwidth at higher power. We could achieve maximum fundamental mode-locking power of 0.934 W at 168 fs pulse duration, corresponding to FWHM bandwidth of  $\sim 35$  nm [see Figs. 7(a) – 7(b)] and TBP of 0.317 ( $1.0\times$  ideal  $\text{sech}^2$ ). At this power level, the intracavity pulse fluence on the SESAM is estimated to be  $\sim 109 \mu\text{J}/\text{cm}^2$ . At this high fluence level we did not observe any damage on this SESAM either and a long-term power stability for the laser operation over 3 hours is recorded [Fig. 7(c)] with a long-term drift of rms  $< 0.3\%$  (over 3 hours) and a short-term drift of rms  $< 0.2\%$  (over 20 min). Due to high intracavity GDD, the soliton mode-locking starts at rather high output power  $\sim 600$  mW. The cavity generates transform-limited pulses throughout the mode-locking range, even without the external GDD compensation [Fig. 7(a)]. The sudden fluctuation in bandwidth as well as in  $\tau_p$  [Fig. 7(a)] is resulting from the fluctuation in central lasing wavelength as discussed previously. A clean RF spectrum is measured, however, not shown here.

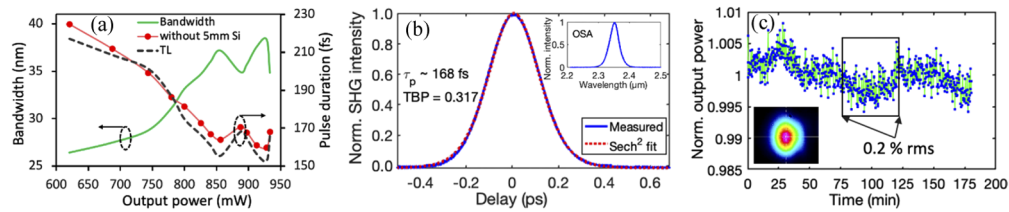


**Fig. 7.** Config-II-b: fundamental mode-locking results using type-II SESAM for highest power output. (a) Measured FWHM bandwidth (green solid), pulse duration (red solid), and estimated ideal transform-limited (TL) pulse duration at corresponding bandwidth (grey dashed) are plotted as a function of output power. (b) Autocorrelation trace with  $\text{sech}^2$  fit. Inset shows optical spectrum of FWHM  $\sim 35$  nm. (c) Output power stability over 3 hours. The rms power fluctuation over indicated (black square) time window is 0.2%. Inset shows measured beam profile.

#### 4.3. Discussion

The laser is operated in the middle of first stability zone, self-starting operation is observed consistently, and mode-locking only occurs with a SESAM present, which indicates that KLM is not responsible for the mode-locking. The low-loss of the SESAMs enables watt-level output power even with only a 5% output coupler, without any noticeable damage on the SESAMs. However, at this high intracavity power level the Cr:ZnS gain element shows strong thermal lensing effect, which we confirm by examining the cavity in cw configuration. Due to polycrystalline structure (grain size comparable to the laser and pump spot size) and Brewster angle cut, the gain element might exhibit non-uniform and non-symmetric heat distribution, which causes the misalignment of the cavity when ramping up the power. Thus, we have adjusted the x-y translation position of the gain element (orthogonal to the cavity length), mainly at higher power, to optimize the mode-locking quality and output power. Note here, a similar result is achieved by tip-tilting any cavity mirror as well. In the case of type-II SESAM, the additional slow recovery time (ns-scale) increases the competition of cw gain in comparison to the mode-locking gain and thus the Cr:ZnS mount is adjusted even at lower power level to get stable mode-locking operation. Nevertheless, the mode-locking is observed over a broad range of output power, and for each case the stability is recorded for hours. Furthermore, we have tested the self-starting nature of the mode-locking by inserting a beam-block in the cavity and observe immediate formation of mode-locked state after opening the beam path.

In general, the best fundamental mode-locking operation is realized for intracavity fluence on SESAMs near the roll-over point (see Fig. 1). Above that harmonic mode-locking is observed with output power crossing 1.2 W. The laser parameters are listed in Table 2. The fast recovery time of the SESAMs (100's fs range) plays a crucial role in both self-starting and stabilizing the mode-locking. In fact, such fast recovery is favoring sub-100-fs pulse formation directly from a SESAM mode-locked oscillator. One may argue that, the higher  $\Delta R$  of the type-II SESAM ( $\sim 3\times$  of type-I) should support shorter pulses, however, as only the fast recovery is contributing here, the effective  $\Delta R$  of type-II SESAM in terms of laser operation is much lower and comparable to that of the type-I SESAM. The achievable shortest pulse duration is mostly limited by the SESAM's finite reflectivity bandwidth and higher orders of dispersion effect. Moreover, for sub-100-fs pulses the effective  $F_2$  parameter associated with inverse saturable absorption is expected to decrease due to stronger multiphoton absorption, which could also limit the output power. The temperature stability of the SESAM is tested by varying the temperature set point of the TEC mount. A stable mode-locking is observed over 10  $\sim$  35°C, with reduction in power at higher temperature due to increasing SESAM absorption loss.

**Table 2. Parameters of SESAM mode-locked fs-250 MHz Cr:ZnS oscillator at ~ 2.37  $\mu\text{m}$  using 5% OC**

Parameters	Type-I SESAM		Type-II SESAM	
	Config-I-a	Config-I-b	Config-II-a	Config-II-b
Pump power (W)	5.6	6.0	5.3	7.5
Output power (W)	0.8	0.96	0.75	0.93
Pulse duration (fs)	79	120	87	168
Bandwidth (nm)	71	50	71	35
Pulse energy (nJ)	3.1	3.9	3.0	3.7
Peak power (kW)	39	32	34.5	22

On the one hand, the InAs/GaSb based type-II multi-QW SESAM structure is ideal for wavelength tunability covering a broad mid-IR range (2–4.5  $\mu\text{m}$ ), have lower strain, and can be grown of high crystal quality with ultralow loss (<0.5%). The only remaining issue is the slow recovery time which hinders the stability and limits the repetition rate. Further investigation is needed at this point. On the other hand, ternary InGaSb/GaSb based type-I QW shows remarkable SESAM parameters. Although such SESAMs exhibit increased strain with higher indium content, our results demonstrate that this strain can be controlled sufficiently well to achieve state-of-the-art laser performance. Moreover, it may be possible to reduce the strain in the future with a quaternary QW structure.

## 5. Conclusion

In conclusion, by developing an ultrafast and low-loss GaSb-based semiconductor saturable absorber mirror (SESAM), we overcome the long-standing issue of power scaling the traditional femtosecond (fs) SESAM mode-locked mid-IR oscillators. We demonstrate record high average output power of 0.96 W for any SESAM mode-locked sub-GHz oscillator delivering 120 fs pulses directly at the 2.37  $\mu\text{m}$  wavelength. This corresponds to pulse energy of ~ 3.9 nJ with peak power of 32 kW. The power is achieved using only a 5% output coupler, which shows the potential of further power scaling to multi-watt level using higher output coupling rates. We used a standard X-fold cavity geometry of low footprint maintaining a low intracavity loss without using any special optics for higher order dispersion management, and the cavity can be easily scalable for different repetition rates. In the same laser cavity, by only altering the pulse fluence on SESAM, we could achieve < 80 fs pulses (> 70 nm of FWHM bandwidth) at a substantial output power of ~ 0.8 W, which was not possible for any SESAM mode-locked mid-IR oscillator until now. To enable these results, we have grown SESAMs of two different absorber profiles, one is InGaSb/GaSb based type-I quantum well (QW) and the other is a InAs/GaSb based type-II multi-QW structure. To the best of our knowledge, this is the first report and use of a type-I SESAM for mode-locking any ultrafast laser at this longer infrared wavelength. Both SESAMs (type-I and type-II) exhibited a sub-picosecond timescale for the initial fast recovery, but very different “slow” recovery timescales. The type-I SESAM had <1.9 ps recovery, which enabled the highest performance. In contrast, for the type-II SESAM the slow timescale was >1 ns, meaning that only 42% of the full modulation depth (corresponding to fast recovery) could contribute to mode-locking. However, the type-II SESAM exhibits lower losses (0.5%) and lower strain. Hence, despite its slower recovery, we could still achieve high performance with the device: 87 fs at 0.75 W in one configuration, and 168 fs at 0.93 W in another. The polycrystalline Cr:ZnS gain element serves an excellent platform for both power and bandwidth scalability beyond the results reported herein. For example, shorter pulses have been generated from Cr:ZnS(e) oscillators either using KLM (34 fs, 50 MHz, 800 mW, OC rate 25% [37]) or Graphene saturable absorber (42.8 fs, 240 MHz, 75 mW, OC rate 1.8% [38]). On the other hand,

the efficiency can be improved by reducing the thermal load on the gain element considering a higher output coupler and improving heat extraction mechanism. Researchers have demonstrated up to 1.9 W of average output power using a high OC rate of 50% [39]. A sophisticated dispersion management, e.g., using customize dispersive mirrors and by flattening the SESAM dispersion profile, will further shorten the laser pulses. Furthermore, a closed box setup together with nitrogen purging would improve the lasing stability for long-term operation.

This high-peak-power mode-locked 2.37- $\mu\text{m}$  laser is well suited for efficient nonlinear frequency conversion processes, such as broadband mid-IR fiber-based [40] and on-chip [3] supercontinuum generation, optical parametric amplification/oscillation [4,8] to reach the long-wave infrared molecular fingerprint spectral region. Moreover, pulses from such 2.4- $\mu\text{m}$  oscillator can be amplified efficiently and compressed sufficiently to be useful in strong-field physics experiments [5]. The wide spectral coverage [ $\sim 200$  nm, see Fig. 4(d)] with sub-watt power level is an excellent light source for direct laser illuminated broadband ultrafast spectroscopy of functional groups, e.g., N-H, C-O, C-H bonds, in the water-free 2 – 2.6  $\mu\text{m}$  atmospheric window. The demonstrated laser paves the way towards industrial standard SESAM mode-locked short-wave infrared oscillators, suitable for both power and repetition rate scaling.

**Funding.** European Research Council (ERC advanced grant 787097 ONE-MIX).

**Acknowledgments.** We thank Dr. V. Wittwer of U. of Neuchatel for providing the IBS coating on the output coupler. We thank FIRST clean room facility of ETH Zurich. A.B. thanks Dr. B. Willenberg of ETH Zurich for useful discussion in the lab.

**Disclosures.** The authors declare no conflicts of interest.

## References

1. K. Scholle, S. Lamrini, P. Koopmann, and P. Fuhrberg, "2  $\mu\text{m}$  Laser Sources and Their Possible Applications," in *Frontiers in Guided Wave Optics and Optoelectronics*, B. P. Pal, ed. (IntechOpen, 2010).
2. N. M. Fried, "Recent advances in infrared laser lithotripsy [Invited]," *Biomed. Opt. Express* **9**(9), 4552–4568 (2018).
3. D. Grassani, E. Tagkoudi, H. Guo, C. Herkommer, F. Yang, T. J. Kippenberg, and C.-S. Brès, "Mid infrared gas spectroscopy using efficient fiber laser driven photonic chip-based supercontinuum," *Nat. Commun.* **10**(1), 1553 (2019).
4. D. Sanchez, M. Hemmer, M. Baudisch, S. L. Cousin, K. Zawilski, P. Schunemann, O. Chalus, C. Simon-Boisson, and J. Biegert, "7  $\mu\text{m}$ , ultrafast, sub-millijoule-level mid-infrared optical parametric chirped pulse amplifier pumped at 2  $\mu\text{m}$ ," *Optica* **3**(2), 147–150 (2016).
5. V. E. Leshchenko, B. K. Talbert, Y. H. Lai, S. Li, Y. Tang, S. J. Hageman, G. Smith, P. Agostini, L. F. DiMauro, and C. I. Blaga, "High-power few-cycle Cr:ZnSe mid-infrared source for attosecond soft x-ray physics," *Optica* **7**(8), 981–988 (2020).
6. V. Petrov, "Frequency down-conversion of solid-state laser sources to the mid-infrared spectral range using non-oxide nonlinear crystals," *Prog. Quantum Electron.* **42**, 1–106 (2015).
7. P. G. Schunemann, K. T. Zawilski, L. A. Pomeranz, D. J. Creeden, and P. A. Budni, "Advances in nonlinear optical crystals for mid-infrared coherent sources," *J. Opt. Soc. Am. B* **33**(11), D36–D43 (2016).
8. K. L. Vodopyanov and P. G. Schunemann, "Broadly tunable noncritically phase-matched ZnGeP<sub>2</sub> optical parametric oscillator with a 2- $\mu\text{J}$  pump threshold," *Opt. Lett.* **28**(6), 441–443 (2003).
9. C. Gaida, M. Gebhardt, T. Heuermann, F. Stutzki, C. Jauregui, J. Antonio-Lopez, A. Schülzgen, R. Amezcua-Correa, A. Tünnermann, I. Pupeza, and J. Limpert, "Watt-scale super-octave mid-infrared intrapulse difference frequency generation," *Light: Sci. Appl.* **7**(1), 94 (2018).
10. S. Vasilyev, I. S. Moskalev, V. O. Smolski, J. M. Peppers, M. Mirov, A. V. Muraviev, K. Zawilski, P. G. Schunemann, S. B. Mirov, K. L. Vodopyanov, and V. P. Gapontsev, "Super-octave longwave mid-infrared coherent transients produced by optical rectification of few-cycle 25- $\mu\text{m}$  pulses," *Optica* **6**(1), 111–114 (2019).
11. I. T. Sorokina, "Cr<sup>2+</sup>-doped II–VI materials for lasers and nonlinear optics," *Opt. Mater.* **26**(4), 395–412 (2004).
12. S. B. Mirov, I. S. Moskalev, S. Vasilyev, V. Smolski, V. V. Fedorov, D. Martyshkin, J. Peppers, M. Mirov, A. Dergachev, and V. Gapontsev, "Frontiers of Mid-IR Lasers Based on Transition Metal Doped Chalcogenides," *IEEE J. Sel. Top. Quantum Electron.* **24**(5), 1–29 (2018).
13. S. Vasilyev, I. Moskalev, M. Mirov, V. Smolski, S. Mirov, and V. Gapontsev, "Ultrafast middle-IR lasers and amplifiers based on polycrystalline Cr:ZnS and Cr:ZnSe," *Opt. Mater. Express* **7**(7), 2636–2650 (2017).
14. S. Vasilyev, I. Moskalev, M. Mirov, S. Mirov, and V. Gapontsev, "Multi-Watt mid-IR femtosecond polycrystalline Cr<sup>2+</sup>:ZnS and Cr<sup>2+</sup>:ZnSe laser amplifiers with the spectrum spanning 1616–26  $\mu\text{m}$ ," *Opt. Express* **24**(2), 1616–1623 (2016).
15. E. Sorokin, N. Tolstik, K. I. Schaffers, and I. T. Sorokina, "Femtosecond SESAM-modelocked Cr:ZnS laser," *Opt. Express* **20**(27), 28947–28952 (2012).

16. M. N. Cizmeciyan, J. W. Kim, S. Bae, B. H. Hong, F. Rotermund, and A. Sennaroglu, "Graphene mode-locked femtosecond Cr:ZnSe laser at 2500 nm," *Opt. Lett.* **38**(3), 341–343 (2013).
17. C. R. Pollock, N. A. Brilliant, D. Gwin, T. J. Carrig, W. J. Alford, J. B. Heroux, W. I. Wang, I. Vurgaftman, and J. R. Meyer, "Mode locked and Q-switched Cr:ZnSe laser using a Semiconductor Saturable Absorbing Mirror (SESAM)," in *Advances Solid-State Photonics, Technical Digest* (Optical Society of America, 2005), paper TuA6.
18. U. Keller, K. J. Weingarten, F. X. Kartner, D. Kopf, B. Braun, I. D. Jung, R. Fluck, C. Honninger, N. Matuschek, and J. A. der Au, "Semiconductor saturable absorber mirrors (SESAM's) for femtosecond to nanosecond pulse generation in solid-state lasers," *IEEE J. Sel. Top. Quantum Electron.* **2**(3), 435–453 (1996).
19. N. Nagl, S. Gröbmeyer, V. Pervak, F. Krausz, O. Pronin, and K. F. Mak, "Directly diode-pumped, Kerr-lens mode-locked, few-cycle Cr:ZnSe oscillator," *Opt. Express* **27**(17), 24445–24454 (2019).
20. Y. Wang, T. T. Fernandez, N. Coluccelli, A. Gambetta, P. Laporta, and G. Galzerano, "47-fs Kerr-lens mode-locked Cr:ZnSe laser with high spectral purity," *Opt. Express* **25**(21), 25193–25200 (2017).
21. S. Vasilyev, I. Moskalev, M. Mirov, S. Mirov, and V. Gapontsev, "Three optical cycle mid-IR Kerr-lens mode-locked polycrystalline Cr<sup>2+</sup>:ZnS laser," *Opt. Lett.* **40**(21), 5054–5057 (2015).
22. M. Guina, A. Rantamäki, and A. Härkönen, "Optically pumped VECSELs: review of technology and progress," *J. Phys. D: Appl. Phys.* **50**(38), 383001 (2017).
23. A. S. Mayer, C. R. Phillips, and U. Keller, "Watt-level 10-gigahertz solid-state laser enabled by self-defocusing nonlinearities in an aperiodically poled crystal," *Nat. Commun.* **8**(1), 1673 (2017).
24. F. Saltarelli, I. J. Graumann, L. Lang, D. Bauer, C. R. Phillips, and U. Keller, "Power scaling of ultrafast oscillators: 350-W average-power sub-picosecond thin-disk laser," *Opt. Express* **27**(22), 31465–31474 (2019).
25. C. J. Saraceno, C. Schriber, M. Mangold, M. Hoffmann, O. H. Heckl, C. R. E. Baer, M. Golling, T. Südmeyer, and U. Keller, "SESAMs for High-Power Oscillators: Design Guidelines and Damage Thresholds," *IEEE J. Sel. Top. Quantum Electron.* **18**(1), 29–41 (2012).
26. T. Ihn, *Semiconductor Nanostructures: Quantum States and Electronic Transport* (Oxford University Press, 2010).
27. A. Rogalski, P. Martyniuk, and M. Kopytko, "InAs/GaSb type-II superlattice infrared detectors: Future prospect," *Appl. Phys. Rev.* **4**(3), 031304 (2017).
28. I. T. Sorokina and E. Sorokin, "Femtosecond Cr<sup>2+</sup>-Based Lasers," *IEEE J. Sel. Top. Quantum Electron.* **21**(1), 273–291 (2015).
29. O. Okhotnikov, A. Grudinin, and M. Pessa, "Ultra-fast fibre laser systems based on SESAM technology: new horizons and applications," *New J. Phys.* **6**(1), 177 (2004).
30. A. Härkönen, C. Grebing, J. Paajaste, R. Koskinen, J.-Alanko, S. Suomalainen, G. Steinmeyer, and M. Guina, "Modelocked GaSb disk laser producing 384 fs pulses at 2 μm wavelength," *Electron. Lett.* **47**(7), 454–456 (2011).
31. M. Haiml, R. Grange, and U. Keller, "Optical characterization of semiconductor saturable absorbers," *Appl. Phys. B* **79**(3), 331–339 (2004).
32. R. Grange, M. Haiml, R. Paschotta, G. J. Spühler, L. Krainer, M. Golling, O. Ostinelli, and U. Keller, "New regime of inverse saturable absorption for self-stabilizing passively mode-locked lasers," *Appl. Phys. B* **80**(2), 151–158 (2005).
33. D. J. H. C. Maas, A.-R. Bellancourt, M. Hoffmann, B. Rudin, Y. Barbarin, M. Golling, T. Südmeyer, and U. Keller, "Growth parameter optimization for fast quantum dot SESAMs," *Opt. Express* **16**(23), 18646–18656 (2008).
34. F. X. Kurtner, J. A. der Au, and U. Keller, "Mode-locking with slow and fast saturable absorbers-what's the difference?" *IEEE J. Sel. Top. Quantum Electron.* **4**(2), 159–168 (1998).
35. A. Krier, ed., *Mid-Infrared Semiconductor Optoelectronics, Springer Series in Optical Sciences* (Springer-Verlag, 2006).
36. F. X. Kartner, I. D. Jung, and U. Keller, "Soliton mode-locking with saturable absorbers," *IEEE J. Sel. Top. Quantum Electron.* **2**(3), 540–556 (1996).
37. N. Nagl, S. Grobmeyer, M. Potzlberger, V. Pervak, F. Krausz, F. Krausz, and K. F. Mak, "Directly Diode-Pumped Few-Optical-Cycle Cr:ZnS Laser at 800 mW of Average Power," in *Conference on Lasers and Electro-Optics, Technical Digest* (Optical Society of America, 2020), paper SF3H.5.
38. N. Tolstik, E. Sorokin, and I. T. Sorokina, "Graphene mode-locked Cr:ZnS laser with 41 fs pulse duration," *Opt. Express* **22**(5), 5564–5571 (2014).
39. S. Vasilyev, M. Mirov, and V. Gapontsev, "Mid-IR Kerr-Lens Mode-Locked Polycrystalline Cr<sup>2+</sup>:ZnS Laser with 0.5 MW Peak Power," in *Advanced Solid State Lasers, Technical Digest* (Optical Society of America, 2015), paper AW4A.3.
40. I. Kubat, C. R. Petersen, U. V. Møller, A. Seddon, T. Benson, L. Brilland, D. Méchin, P. M. Moselund, and O. Bang, "Thulium pumped mid-infrared 0.9–9 μm supercontinuum generation in concatenated fluoride and chalcogenide glass fibers," *Opt. Express* **22**(4), 3959–3967 (2014).